Cooperative polymerization of one-patch colloids

Teun Vissers, Frank Smallenburg, Gianmarco Munaò, Zdenk Preisler, and Francesco Sciortino

Citation: The Journal of Chemical Physics **140**, 144902 (2014); doi: 10.1063/1.4869834
View online: http://dx.doi.org/10.1063/1.4869834
View Table of Contents: http://scitation.aip.org/content/aip/journal/jcp/140/14?ver=pdfcov
Published by the AIP Publishing

Cooperative polymerization of one-patch colloids

Teun Vissers,[a] Frank Smallenburg,[a] Gianmarco Munaò, Zdeněk Preisler, and Francesco Sciortino
Sapienza, Università di Roma, Piazzale Aldo Moro 2, 00185, Roma, Italy

(Received 17 October 2013; accepted 7 March 2014; published online 10 April 2014)

We numerically investigate cooperative polymerization in an off-lattice model based on a pairwise additive potential using particles with a single attractive patch that covers 30% of the colloid surface. Upon cooling, these particles self-assemble into small clusters which, below a density-dependent temperature, spontaneously reorganize into long straight tubes. We evaluate the partition functions of clusters of all sizes to provide an accurate description of the chemical reaction constants governing this process. Our calculations show that, for intermediate sizes, the partition functions retain contributions from two different structures, differing in both energy and entropy. We illustrate the microscopic mechanism behind the complex polymerization process in this system and provide a detailed evaluation of its thermodynamics. © *2014 AIP Publishing LLC*. [http://dx.doi.org/10.1063/1.4869834]

I. INTRODUCTION

The formation of one-dimensional aggregates from a system composed of identical monomers is a process of paramount importance in biology, chemistry, material science and physics, and continues to receive significant attention. Such structures arise spontaneously under appropriate external conditions, and can be found in many systems, e.g., synthetic polymer molecules,[1–4] carbon nanotubes,[5,6] amyloid fibers,[7,8] tubular surfactant micelles,[9,10] DNA wires,[11,12] and colloidal chains.[13,14] A special example is the so-called "equilibrium polymerization" (sometimes also called supramolecular polymerization), where the monomers associate via reversible interactions, i.e., in the absence of covalent bonds.[15–20] Equilibrium polymerization processes giving rise to one-dimensional aggregates are commonly classified in two broad classes: isodesmic polymerization[17,18] and cooperative polymerization (CP).[21–24] In the first class, the free-energy change on bonding is essentially independent of the polymer size. Theoretical modeling of one-dimensional polymerization predicts that this type of aggregation results in an exponentially polydisperse distribution of polymer lengths, with an average length that changes smoothly upon varying density and temperature.[18,25–33] In dilute conditions, parameter-free theoretical predictions[14,18,28–30] properly describe the assembly process even in the limit of strong association, when the average length is much larger than one.

In the case of cooperative polymerization, the growth of the polymer typically consists of multiple stages in which several building blocks combine into a secondary structure that then grows out.[21–24] Such a transition typically occurs much more sudden than in isodesmic growth and in some cases strongly resembles a first-order transition.[21,24,34,35] In addition, sometimes a competition between several supramolecular polymer structures is present.[36–39] In the case of sulfur, a well known example of CP, the polymerization involves existing S_8 ring-structures of sulfur that break open and then connect to form polymer chains.[40–43] We note in passing that equilibria involving rings and polymers can be mapped onto the problem of Bose-Einstein condensation.[44]

Cooperative polymerization mechanisms have also been identified for filaments formed by biologically relevant organic compounds such as actin[45] and guanosine,[46,47] and in the formation of amyloid fibers.[8] In CP, the average chain length almost abruptly varies from small to large values upon a small change in density and/or temperature. Modeling of CP is often based on the assumption of multiple equilibrium constants and then requires some degree of fitting when comparing theoretical predictions to experimental data.[17]

One class of models—commonly referred to after the authors as Kern-Frenkel (KF) models,[48] having its origin in the work of Bol[49]—has received notable attention in recent years as a convenient implementation for so-called "patchy" colloidal particles, i.e., colloids of a new generation that interact anisotropically via specific spots on their surface. In these models, attractive patches are characterized by a directional square-well potential combined with a spherical hard-core repulsion. This strategy has proven valuable for describing key phenomena exhibited by these particles, such as the gas-liquid phase separation[50–52] and the formation of crystals[53–58] and other organized structures.[59–63] Recently, we have employed such KF models to study the phase behavior of one-patch particles with varying surface coverage. For the case of 30% attractive surface, we discovered[64,65] the sudden formation of extremely long tubular structures self-assembling at specific temperatures and densities, suggestive of CP. We note here that also other patch potentials can result in fibers and bundles. One example is given by Huisman *et al.*,[35] who use an anisotropic Lennard-Jones-based potential to model two-patch particles. The choice of this specific potential strongly favors a head-to tail alignment of the particles, leading to the formation of one-dimensional chains. Because there is also a weak attraction when the particles are not perfectly aligned, the formed chains also attract each other sideways and assemble into bundles.

[a]T. Vissers and F. Smallenburg contributed equally to this work.

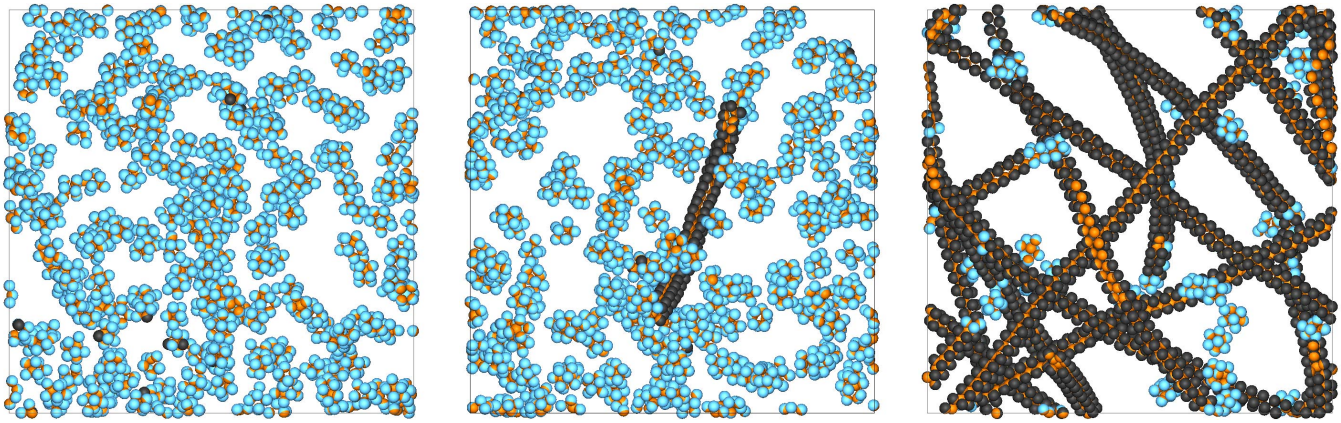

FIG. 1. Snapshots of constant NVT simulations, for $k_BT/\epsilon = 0.145$ (a), $k_BT/\epsilon = 0.14$ (b), and $k_BT/\epsilon = 0.13$ (c), all at density $\rho\sigma^3 = 0.05$. The attractive hemispheres are depicted in orange. Particles in a tube-like environment, according to the order parameter in Eqs. (5) and (6), are labeled black/orange. Other particles are blue/orange.

An important step in colloidal physics which has relevance to polymerizing systems is the recent development of accurate numerical methodologies for evaluating the partition function of clusters of different sizes.[66–68] From this information, the relative free energies of clusters consisting of different numbers of particles can be calculated, providing a transparent route for evaluating the equilibrium constant of all "reactions" between clusters. In this article, we apply this new methodology, complemented with standard Monte Carlo simulations, to perform an in-depth investigation of the polymerization process in the KF[48] one-patch model with 30% surface coverage. We show that this model indeed constitutes an example of cooperative polymerization, in which the particles themselves are the smallest building blocks. In contrast to some molecular systems, these particles do not change shape or conformation. In addition, we provide a detailed description of the self-assembly process by numerically evaluating the cluster partition functions. We observe the onset of polymerization as a crossover from monomers into small disorganized oligomers or clusters. At sufficiently low temperature, we observe a structural transition into rigid tubes for a cluster size of approximately 30–40 monomers. Above these cluster sizes, we never observe disordered clusters and only the rigid tubes are present. We also show that the appearance of the tubes is marked sharply around a critical temperature and density.

II. MODEL

To model the interactions between patchy particles we employ the well-known one-patch Kern-Frenkel potential,[48] representing a hard-sphere colloid in which one spherical cap of the particle surface has been functionalized to become attractive when facing the spherical cap of a neighboring particle. The KF potential can be described as follows:

$$u^{\mathrm{KF}}(\mathbf{r}_{ij}, \hat{\mathbf{n}}_i, \hat{\mathbf{n}}_j) = u^{\mathrm{SW}}(r_{ij})\Omega(\mathbf{r}_{ij}, \hat{\mathbf{n}}_i, \hat{\mathbf{n}}_j) + u^{\mathrm{HS}}(r_{ij}). \quad (1)$$

The term $u^{\mathrm{SW}}(r_{ij})$ describes the square-well interaction potential

$$u^{\mathrm{SW}}(r_{ij}) = \begin{cases} -\epsilon & \text{if } \sigma < r_{ij} \le \sigma + \Delta \\ 0 & \text{otherwise,} \end{cases} \quad (2)$$

where σ is the particle diameter, $\Delta = 0.5\,\sigma$ is the interaction range, and ϵ is the well depth. $\Omega(\mathbf{r}_{ij}, \hat{\mathbf{n}}_i, \hat{\mathbf{n}}_j)$ is a function that depends on the orientations of the two interacting particles

$$\Omega(\mathbf{r}_{ij}, \hat{\mathbf{n}}_i, \hat{\mathbf{n}}_j) = \begin{cases} 1 & \text{if } \begin{cases} \hat{\mathbf{r}}_{ij} \cdot \hat{\mathbf{n}}_i > \cos\theta & \text{and} \\ \hat{\mathbf{r}}_{ji} \cdot \hat{\mathbf{n}}_j > \cos\theta \end{cases} \\ 0 & \text{otherwise,} \end{cases} \quad (3)$$

where $\hat{\mathbf{n}}_i$ and $\hat{\mathbf{n}}_j$ denote the orientations of the patch centers of particles i and j, respectively, and $\mathbf{r}_{ij}$ is the vector joining the center of mass of the two particles. We also set the patch coverage fraction $\chi = 0.3$ which corresponds to a patch opening angle $\cos\theta = 0.4$. Finally, the hard-sphere potential $u^{\mathrm{HS}}(r_{ij})$ guarantees that particles do not overlap

$$u^{\mathrm{HS}}(r_{ij}) = \begin{cases} \infty & \text{if } r_{ij} \le \sigma \\ 0 & \text{otherwise.} \end{cases} \quad (4)$$

III. RESULTS

A. The formation of tubular structures

Self-assembly takes place usually at low temperatures (as compared to the bonding energy) and simulating such systems intrinsically requires extremely long simulations and careful analysis of the equilibration process. Standard NVT simulations with a constant number of particles ($N = 2000$ for these simulations), volume V and temperature T can provide insights into the structure of the system. An analysis of the NVT configurations shows that the present system forms increasingly larger aggregates, which then transform into well-defined one-dimensional tube-like structures below a density-dependent crossover temperature T_x. Figs. 1(a)–1(c) provide snapshots of the system just above, around, and just below T_x. While for $T > T_x$, the system is composed of small aggregates, for $T < T_x$ a significant share of the particles is part of a limited number of long tubular structures.

In order to quantify the tube formation process, we have devised a single-particle order-parameter which is able to discriminate between the local environment of particles in tubes and in all other geometries. From analyzing the environment of particles in tubes, we found that (for this specific model) a

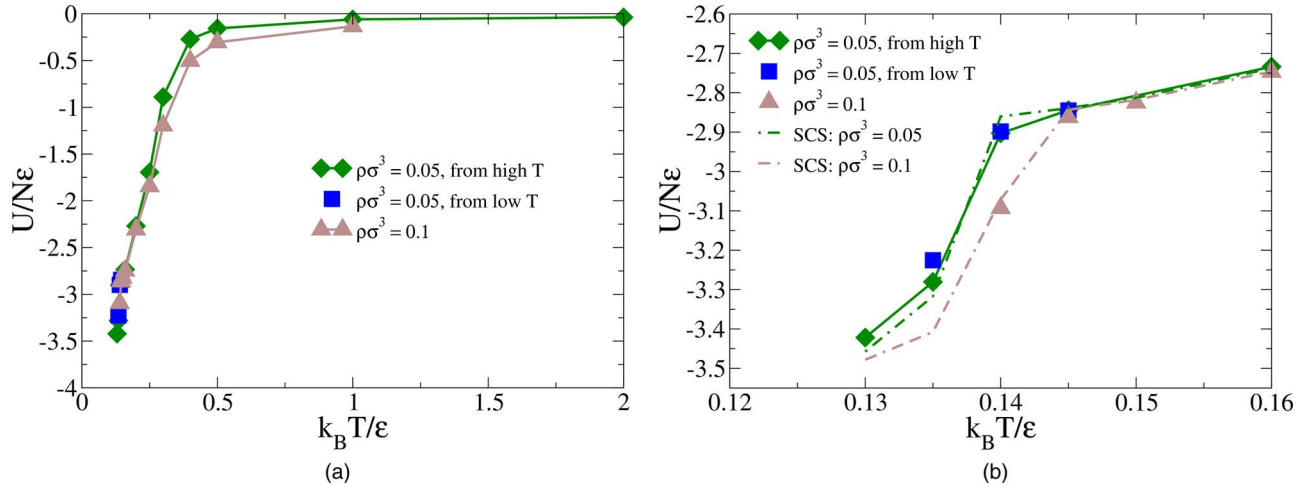

FIG. 2. (a) Temperature dependence of the potential energy for two different densities $\rho\sigma^3 = 0.05$ and $\rho\sigma^3 = 0.1$ as obtained by simulations at constant NVT (b) Close-up depicting the crossover region and comparison between MC NVT results (symbols) and single-cluster simulations (SCS; dashed-dotted lines).

particle i inside a tube has exactly 7 bonds with neighboring particles (labeled j). Using the orientations $\hat{\mathbf{n}}_i$ and $\hat{\mathbf{n}}_j$ of the particle i and j, respectively (as defined in Eq. (3)), two out of the seven bonds are characterized by

$$\hat{\mathbf{n}}_i \cdot \hat{\mathbf{n}}_j < -0.85, \tag{5}$$

while the remaining five satisfy

$$-0.65 < \hat{\mathbf{n}}_i \cdot \hat{\mathbf{n}}_j < 0.65. \tag{6}$$

The first two represent bonds with nearby particles pointing almost exactly in the opposite direction, and the other five bonds are with particles oriented neither parallel nor anti-parallel. Particles with seven bonded neighbors satisfying the relations in Eqs. (5) and (6) are defined as tube-like particles and are marked accordingly in Fig. 1.

The presence of a sharp crossover temperature is revealed by the T-dependence of the potential energy U. Fig. 2 shows U as a function of T for several densities. The potential energy clearly shows a "kink" at a well-defined temperature T_x, below which its value decreases sharply, approaching the limiting value of seven bonds ($U/N\epsilon = -3.5$) per particle, which would be reached for infinitely long tubes.

To provide evidence that the reported energies are equilibrium values, we show in Fig. 2 the potential energy evaluated from NVT-MC simulations with differing starting conditions: one in which the initial configuration was comprised of distinct monomers and one from a configuration of preformed tubes. Convergence of the energy of the two simulations (from monomers and from tubes) to the same equilibrium value is presented as evidence of thermal equilibration.

B. Cluster partition function: Single-cluster method

The aggregation process under scrutiny can be already observed at low densities, where the system can be approximated as a collection of non-interacting clusters. This offers the possibility to study the system as a distribution of clusters of various size, which gives direct information about the structure of the system. Under dilute conditions, the Helmholtz free energy $F(N, V, T)$ can be approximated by that of an ideal gas of clusters,

$$\beta F(N, V, T) = \sum_{n=1}^{\infty} N_n[\log N_n - 1 - \log \mathcal{Z}_n], \tag{7}$$

where $\beta = 1/k_B T$ with k_B Boltzmann's constant, N_n is the number of clusters of size n, and $\mathcal{Z}_n$ is the partition function of a cluster of size n, given by

$$\mathcal{Z}_n = \frac{1}{(4\pi)^n \Lambda^{3n} n!} \int_V d\mathbf{r}^n \int d\hat{\mathbf{n}}^n e^{-\beta U(\mathbf{r}^n, \hat{\mathbf{n}}^n)} c(\mathbf{r}^n, \hat{\mathbf{n}}^n). \tag{8}$$

Here, $\mathbf{r}^n$ and $\hat{\mathbf{n}}^n$ denote the positions and orientations of the particles, respectively. The thermal volume Λ^3 does not affect the thermodynamic behavior of the system, and can therefore be chosen to be equal to a unit volume $\Lambda^3 = \sigma^3$.

The function $c(\mathbf{r}^n, \hat{\mathbf{n}}^n)$ is a constraint function that equals 1 if the n particles form a single continuous cluster, and is 0 otherwise. In the present model, there is no ambiguity in the definition of a bond, as the potential is stepwise. Any pair of particles with interaction energy equal to $-\epsilon$ is considered bonded and part of the same cluster. The integral over the coordinates $\mathbf{r}^n$ can be transformed into an integral over $\mathbf{r}_1$ and over the relative coordinates $\mathbf{r}_j - \mathbf{r}_1$. The first integration generates a volume V term that describes the cluster entropy associated with the exploration of the available volume. From $\mathcal{Z}_n$, one can define a cluster free energy $\beta f_n \equiv -\log \mathcal{Z}_n$, a cluster energy $U_n \equiv -\partial(\beta f_n)/\partial\beta$, and a cluster entropy $S_n/k_B = -\beta f_n + \beta U_n$. For the monomers, $\mathcal{Z}_1 = V/\Lambda^3$, $\beta f_1 \equiv -\log(V/\Lambda^3)$.

The equilibrium cluster size distribution can be calculated by minimizing the free energy with respect to N_n, while satisfying the constraint

$$\sum_n n N_n = N. \tag{9}$$

This yields

$$\frac{N_n}{N_1^n} = \frac{\mathcal{Z}_n}{\mathcal{Z}_1^n}. \tag{10}$$

The partition function $\mathcal{Z}_n$ can be evaluated numerically for any n.[66–68] Here we exploit the methodology outlined in

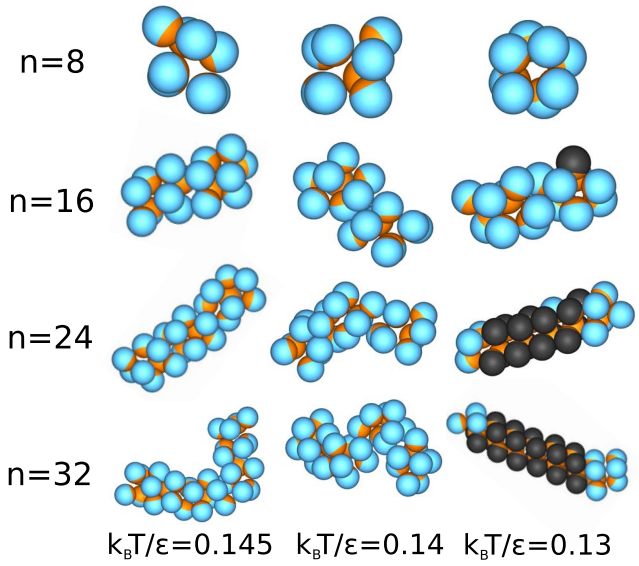

FIG. 3. Typical clusters of size $n = 8$, 16, 24, 32 for three different temperatures above, around, and below T_x, $k_BT/\epsilon = 0.13$, 0.14, and 0.145. Orange hemisphere are attractive. Particles that are tube-like, according to the order parameter in Eqs. (5) and (6), are depicted in black/orange, other particles are blue/orange.

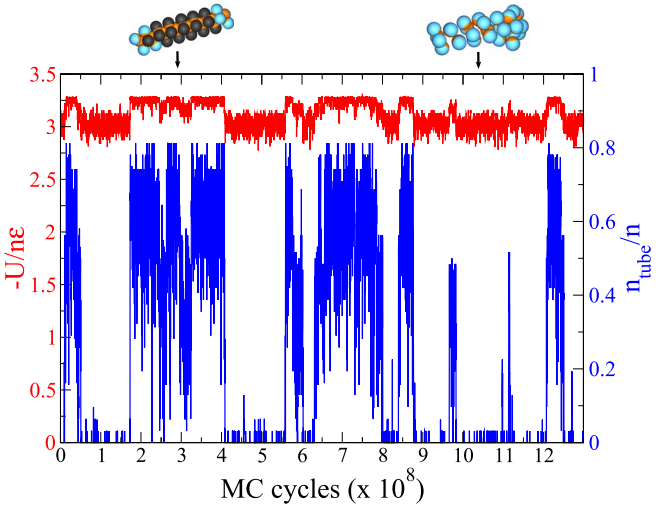

FIG. 4. Evolution of a cluster of size $n = 31$ in a single-cluster simulation, at $k_BT/\epsilon = 0.135$. The red line (top) shows the (negative of the) energy per particle ($-U_n/n\epsilon$), whereas the blue line (bottom) depicts the fraction of tube-like particles in the cluster n_{tube}/n. The conformational change between disorganized clusters and straight tube-like aggregates marks the crossover from clusters to tubes.

Refs. 61 and 68, in which the relations between the various $\mathcal{Z}_n$ can be obtained directly from a grand-canonical Monte Carlo (GCMC) simulation, i.e., a simulation at fixed T, V, and chemical potential μ. The simulation starts with a single cluster and rejects all moves (insertion, deletion, translation, or rotation) in which the system breaks into more than one cluster. By imposing the constraint of simulating only a single cluster, the probability $\mathcal{P}(n)$ of observing a cluster of size n becomes

$$\frac{\mathcal{P}(n)}{\mathcal{P}(1)} = \frac{\mathcal{Z}_n}{\mathcal{Z}_1} e^{\beta\mu(n-1)}. \tag{11}$$

Hence, the ratio $\mathcal{Z}_n/\mathcal{Z}_1$ can be directly obtained for all n from the GCMC simulation. Note that $\mathcal{Z}_n/\mathcal{Z}_1$ is independent of μ (and of the volume of the simulation box), and therefore one can set $\mu = 0$ in the grand-canonical simulation without loss of generality. With this choice,

$$\frac{\mathcal{Z}_n}{\mathcal{Z}_1} = \frac{\mathcal{P}(n)}{\mathcal{P}(1)}. \tag{12}$$

Since we know $\mathcal{Z}_1 = V/\Lambda^3$, this allows us to use Eq. (10) to directly calculate the cluster size distribution for any density for which the ideal gas of cluster approximation holds.

Note that we have neglected to include cluster-excluded volume interactions in our derivation here. While an approximate correction for these effects can be included in the theory,[61,66] we have omitted this here in order to simplify the derivation, as well as strengthen the ties to molecular polymerization, which typically occurs under dilute conditions. This will lead to a slight discrepancy between single-cluster and NVT simulations at higher densities, where the single-cluster results underestimate the formation of large clusters.

Figure 3 shows snapshots of clusters of different sizes, taken from the single-cluster simulations. Clusters of small size are formed by almost spherical aggregates, with the attractive patches all located near the center of the cluster. Around $n \approx 20$, a well-defined tubular structure appears which competes for stability with other cluster shapes. This low-energy one-dimensional structure becomes dominant for larger n, driving the polymerization process.

In the crossover regime between small clusters and long tubes, two distinct cluster structures compete. Fig. 4 shows the evolution of the energy of a cluster of size $n = 31$ during a single-cluster simulation at a temperature close to T_x. The energy per particle oscillates between two values, corresponding to a tubular state and to other structures, respectively. The correlation between the energy values and the cluster structure is confirmed by the time evolution of the order parameter that tracks the number of particles in a tube-like environment. Similar results are observed in the whole region $20 < n < 33$, suggesting the existence of two well-defined free-energy minima, corresponding to two distinct cluster structures. These two structures are in thermodynamic (chemical) equilibrium. It is the reaction constant of this equilibrium that controls the tube nucleation process which is then followed by the tube polymerization process for larger clusters.

Figure 5 shows the average energy per particle $U_n/n\epsilon$ for clusters of different size n at different T. The lowest-energy clusters are indeed the ones consisting of a large number of particles, i.e. the tubular structures, which appear to be stabilized by energy. Since the interaction potential is modeled via a square-well interaction there is no vibrational component to the energy and the cluster energy is proportional to the number of contacts only. The temperature dependence of the cluster energy can thus be ascribed to the different number of contacts explored at different T.

At low temperatures and for large clusters ($n \gtrsim 30$), the ratio $\mathcal{Z}_{n+1}/\mathcal{Z}_n$ becomes periodic. At this point, clusters are always tube-like, and the free-energy change associated with adding an extra "layer" to a tube does not depend on the length of the tube. In the case of the specific system under considera-

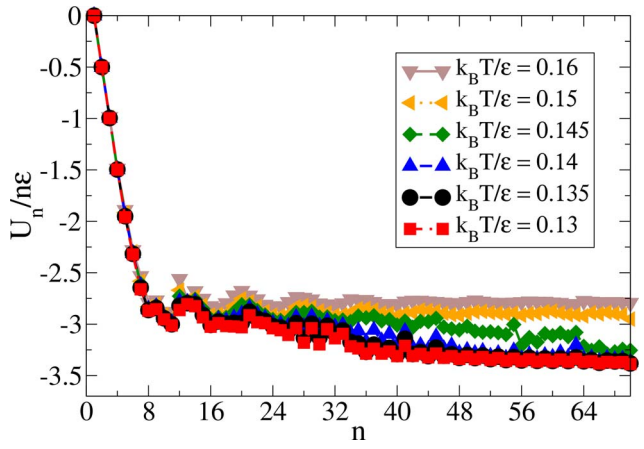

FIG. 5. The average potential energy per particle U_n for a cluster of size n for different temperatures k_BT/ϵ, as obtained in the single-cluster simulations.

tion here, the layer is composed by two particles and $\mathcal{Z}_{n+1}/\mathcal{Z}_n$ oscillates with periodicity 2: the cost of adding a particle to a long tube only depends on whether the current cluster size is even or odd. Therefore, we can easily extrapolate our results to obtain the partition functions $\mathcal{Z}_n$ for much longer tubes than those we studied. For the results shown here, single-cluster simulations were performed up to size $n = 100$. For larger cluster sizes (up to $n = 10\,000$), we separately averaged the even and odd values of $\mathcal{Z}_{n+1}/\mathcal{Z}_n$ over the larger cluster sizes ($45 \leq n \leq 100$), and used these for extrapolation.

C. Modeling of the polymerization process

Next we use information evaluated from the single-cluster partition functions to highlight the aggregation process for different temperatures and densities.

Fig. 6 shows the cluster size distribution at $\rho\sigma^3 = 0.05$ as calculated from the single-cluster simulations method and from the constant NVT simulations. Indeed, using the values of the partition functions at fixed T, we can evaluate the

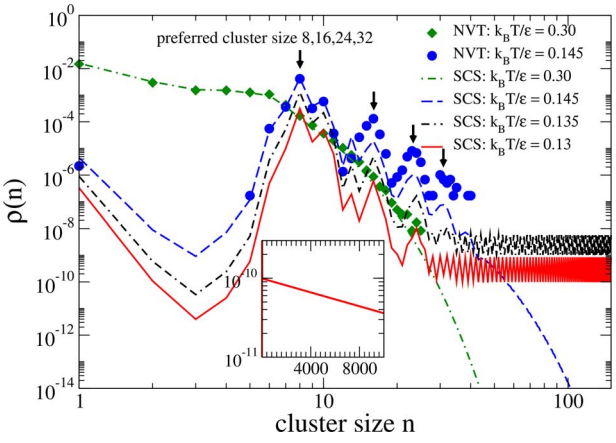

FIG. 6. Cluster size distribution $\rho_n \equiv N_n/V$ at $\rho\sigma^3 = 0.05$ from the NVT simulations and single-cluster simulations. Note that no NVT cluster size distribution is present for $k_BT/\epsilon = 0.13$ since in this case the number of clusters inside the simulation box is so small that a proper averaging of the distribution becomes impossible. The inset shows the exponential decay of the SCS cluster size distribution for larger cluster sizes (only odd points are shown).

cluster size distribution via Eq. (10). Here, N_1 acts as a free parameter that determines the overall system density, via the relation $\sum_n nN_n = N$, where n is the cluster size. At high T, N_n is monotonically and smoothly decaying, indicating the absence of strongly favored cluster sizes: the system consists mainly of clusters of only a few particles. Already above T_x, the cluster size develops a highly non-monotonic character, signaling the presence of preferred cluster sizes ($n = 8$ and its multiples). Still, the largest cluster ever observed in the NVT simulations at this temperature does not exceed $n = 40$. For $T < T_x$ there is an explosion of very long aggregates (the tubes), whose size n extends well beyond 100 particles. For large n, the length distribution from the single-cluster simulations decays exponentially (Fig. 6, inset). For these low T, NVT simulations are not able to provide information on the large n windows due to the finite number of particles ($N = 2000$) in the simulation box. At T for which a comparison between single-cluster simulations and NVT simulations is possible, the two methods provide consistent results.

Fig. 7 shows the T dependence of the clustering and polymerization processes. Upon decreasing the temperature, Fig. 7(a) first shows a crossover from monomers to small clusters. Then, the average cluster size suddenly increases below a well-defined temperature. This change is accompanied by a sudden decrease in the potential energy (Fig. 7(b)), as particles in tubes are bound in a configuration with the maximum number of possible bonds.

Fig. 8 shows the corresponding density dependence. Fig. 8(a) shows the average cluster size and Fig. 8(b) the potential energy per particle as a function of ρ for a given T. Upon increasing the density at a given temperature, first small clusters start to form followed by the sudden formation of tubes. For lower temperatures, the onset of tube-formation occurs already at lower ρ. In this representation, it can be seen again that there is a sudden transition from clusters to tubes at around density ρ_x.

In Fig. 9(a), the points where monomers start combining into small clusters as well as the transition from clusters into tubes are depicted in the $\rho - T$ plane for both constant NVT simulations and single-cluster simulations. For the first crossover, we marked the points where 10% of the particles is in a dimer. For the transition of clusters into tubes, we marked the state points for which 10% of the particles are in a tube-like environment according to Eqs. (5) and (6).

For a polymerization transition, the critical temperature is expected to be proportional to the logarithm of the monomer concentration. In Fig. 9(b), these points are represented in the $\log(\rho)$-$1/T$ plane. Indeed, a linear relation well describes the transition from clusters to tubular aggregates.

It has been noted by Douglas *et al.*[24] that for cooperative polymerization, the average cluster size shows a linear increase with the total particle density. In Fig. 10(a), the average cluster size as a function of the particle density is depicted for our model. Note that in the region where the tubes start to grow, the average cluster size indeed increases linearly with density, indicating cooperative polymerization.

To illustrate the cause of this phenomenon, we calculate the concentration of monomers, octomers, and the total concentration of clusters in our system. Fig. 10(b) shows the

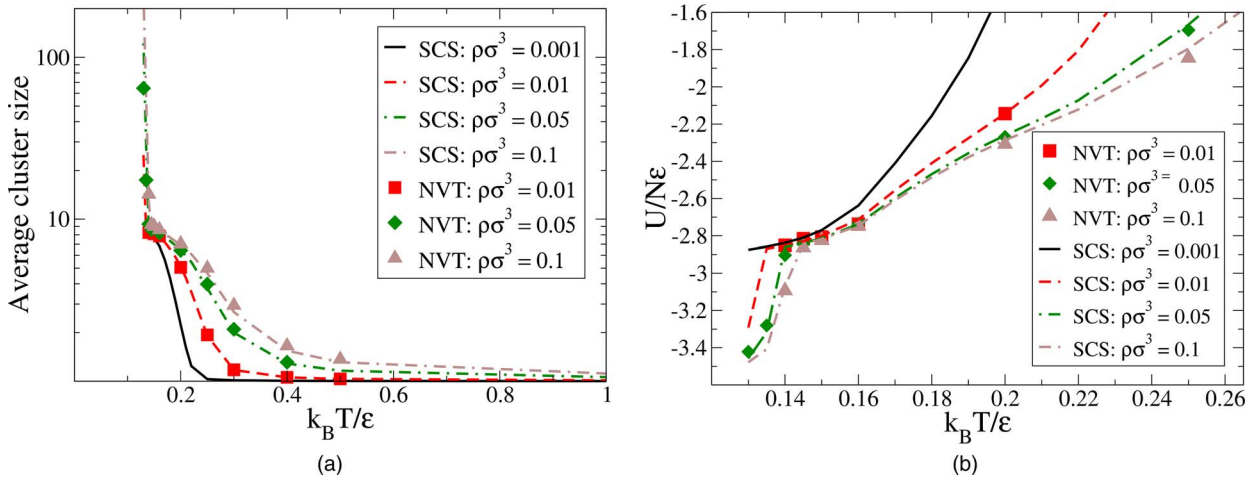

FIG. 7. (a) The average cluster size versus temperature and (b) the energy per particle versus temperature for different densities from NVT simulations (symbols) and single-cluster simulations (lines).

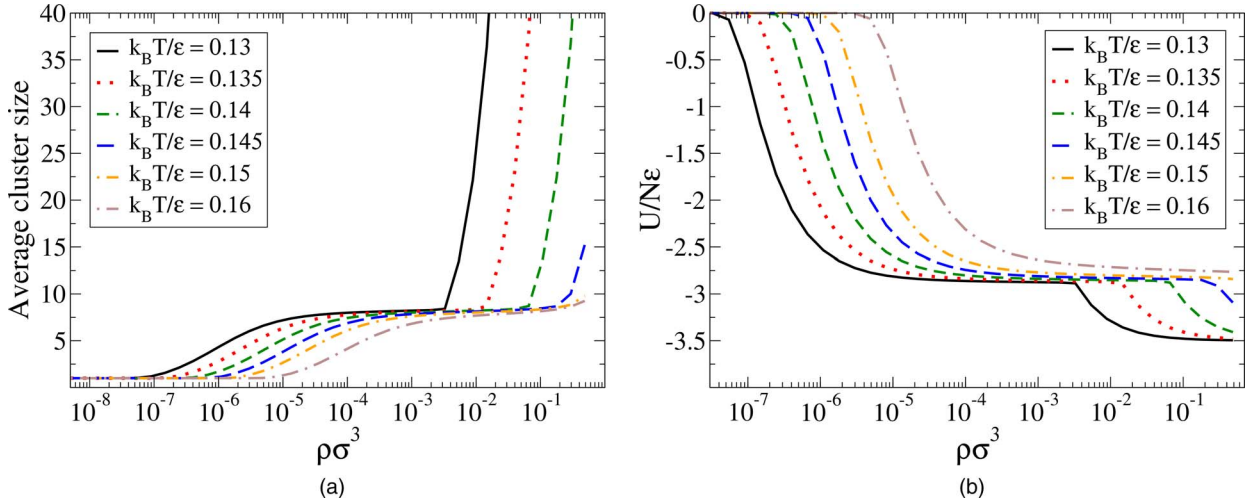

FIG. 8. (a) The average cluster size versus density and (b) the average energy per particle versus density from single-cluster simulations.

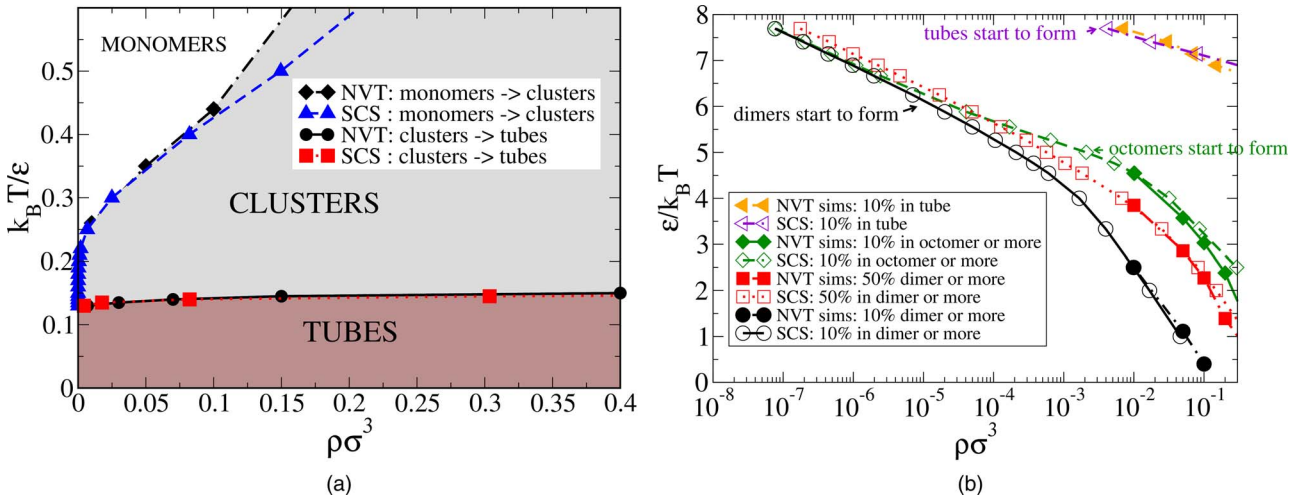

FIG. 9. (a) The crossover from monomers to clusters and the transition from cluster into tubes depicted in the $\rho - T$ plane from constant NVT-simulations and single-cluster simulations. The crossover from monomers to clusters is depicted with points for which 10% of the particles is part of a cluster (black diamonds and blue triangles). The conformational transition from disorganized clusters to straight tubes is marked with black dots, for which 10% of the particles are in a tube-like environment according to Eqs. (5) and (6) (black dots and red squares). (b) Results from the constant NVT simulations and single-cluster simulations plotted in the $\log(\rho) - 1/T$ plane.

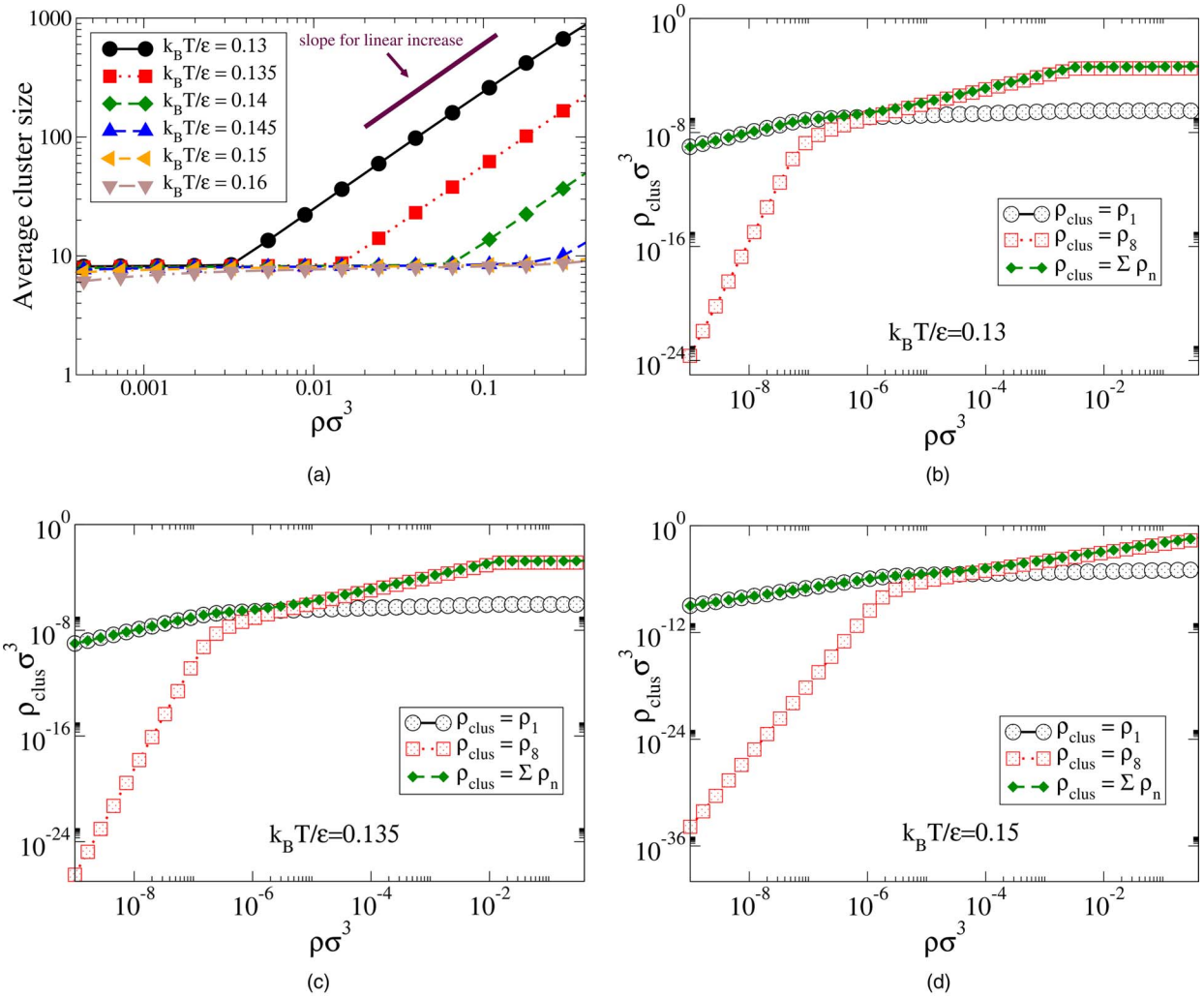

FIG. 10. (a) Same as Fig. 8(a), but on a log-log scale to show the linear increase of the average cluster size with temperature – the maroon line reflects the slope for a perfect linear increase. (b)–(d) Cluster density ρ_{cluster} as a function of density ρ for clusters of size 1 ($\rho_1 \equiv N_1/V$) and 8 ($\rho_8 \equiv N_8/V$) and for the total cluster number density $\sum_n \rho_n$ at temperatures $k_B T/\epsilon = 0.13$, $k_B T/\epsilon = 0.135$, and $k_B T/\epsilon = 0.15$.

density of clusters of size 1 and 8, as well as the total cluster density (i.e., the sum of all ρ_n) for $k_B T/\epsilon = 0.13$. At high densities where tubes form, the majority of clusters are still of size 8, as we can also read from the cluster size distribution in Fig. 6. As a result, the total cluster density is almost constant for the entire range of densities where the tubes form. Since the average cluster size is the density divided by the total cluster density, this causes the linear behavior in the average cluster size shown in Fig 10(a). For higher T, this effect becomes less pronounced (Fig. 10(c)), while at $k_B T/\epsilon = 0.15$ – above the polymerization transition temperature T_x – the clusters remain much smaller and the total cluster density continues to increase with ρ (Fig. 10(d)).

The results shown so far provide clear evidence of a polymerization process which develops quite abruptly below $T_x(\rho)$. In a very short T interval the system structure changes from a fluid of small clusters, with a preferential size of eight units to a fluid of long tubes. This fast onset of a polymerization process is typical for cooperative polymerization, in contrast to the more gradual growth associated with isodesmic polymerization. The present model thus provides a microscopic model for examining the basic ingredients of CP.

Rod-like aggregates are often associated with nematic phases.[12] From earlier work,[65] we know that the tube-phase is – although kinetically preferred – in fact metastable to a coexistence of crystals of aligned tubes with a low-density fluid in a large range of densities. At high densities there is a pocket where a crystal of tubes is stable. As the tubes are effectively long rods, we also expect a (metastable) nematic phase at low temperature and high density. However, due to the very large average length of the tubes, we cannot perform simulations for large densities but only limit ourselves to detect the onset of tube growth. This prevents us from observing the expected transition to a nematic phase on increasing density and/or lowering temperature. Close to T_x, where simulations are still feasible, the system is isotropic.

D. Signature of cooperative polymerization in the reaction constant

In a more chemically oriented approach, the clustering process can be seen as a chemical reaction between clusters of different size. A cluster of size n is then considered the result of the aggregation of n monomers. From Eq. (10), the

relative concentration of monomers $\rho_1 \equiv N_1/V$ and n −mers $\rho_n \equiv N_n/V$ satisfies

$$\frac{\rho_n}{\rho_1^n} = V^{n-1}\frac{\mathcal{Z}_n}{\mathcal{Z}_1^n}. \tag{13}$$

Commonly, one defines an equilibrium constant K_n for this chemical equilibrium (with dimensions of $[V]^{n-1}$),

$$K_n \equiv \frac{\rho_n}{\rho_1^n} = \frac{\mathcal{Z}_n}{\mathcal{Z}_1}\Lambda^{3(n-1)}, \tag{14}$$

where the relation $\mathcal{Z}_1 = \frac{V}{\Lambda^3}$ has been exploited. The quantity K_n has the advantage of visualizing the change in the free energy associated with bonding, separate from the contribution of the free-energy change associated with the loss of translational entropy. Indeed, the V^{n-1} factor in Eq. (13) compensates the entropy loss associated with the exploration of the sample volume by the n monomers (V^n) which, once aggregated, is retained only by the center of mass of the cluster (V). The V-independence of K_n is also clearly seen when expressing it in terms of cluster free energies

$$K_n = \Lambda^{3(n-1)}\frac{e^{-\beta f_n}}{e^{-\beta f_1}} = \Lambda^{3(n-1)}e^{-\beta(f_n - f_1)}. \tag{15}$$

We note here that the inclusion of hard-core repulsions in the free energy in Eq. (7) will lead to equilibrium constants that are dependent on the packing fraction. However, under dilute conditions such corrections will have a negligible effect.

The n-dependence of K_n carries all relevant information for an equilibrium aggregation process. For example, in the case of the isodesmic polymerization all bonds contribute equally to the free-energy of the cluster. As a result, monomers with functionality two bind into chains always with the same free-energy change[18] and

$$e^{-\beta f_n^{\text{isodesmic}}} = \frac{V}{\Lambda^3}\left(\frac{v_b}{\Lambda^3}\right)^{n-1} e^{-\beta(n-1)\Delta U}, \tag{16}$$

where ΔU is a measure of the energy associated with forming a bond, and v_b is the bonding volume, measuring the volume a particle can explore, while bonded to a neighbor. The corresponding equilibrium constant is given by

$$K_n^{\text{isodesmic}} = (v_b e^{-\beta\Delta U})^{n-1} = (K_2^{\text{isodesmic}})^{n-1}. \tag{17}$$

From this relation, we can read directly that

$$\frac{\log(K_n^{\text{isodesmic}}\Lambda^{-3(n-1)})}{(n-1)} = \frac{-\beta(f_n^{\text{isodesmic}} - f_1^{\text{isodesmic}})}{n-1} = \log(v_b\Lambda^{-3}) - \beta\Delta U \tag{18}$$

is independent of n for isodesmic polymerization.

Additionally, we see that $(f_n - f_1)/n$ is a measure for the (negative of) the free energy per particle in a cluster with fixed center of mass.

Fig. 11 shows the n-dependence of $\log(K_n\Lambda^{-3(n-1)})/(n-1)$, calculated according to Eq. (15). For large n ($n \gtrsim 40$), a constant value is reached, confirming that for cooperative polymerization the free-energy change upon adding another number of monomers becomes independent of the cluster size for sufficiently large n, similar to isodesmic models (Eq. (18)). Note, however, that for this model, there is still a small difference based on whether n is odd or even (see inset of Fig. 11) due to the fact that each tube layer is composed by two particles (see tubes in Fig. 3).

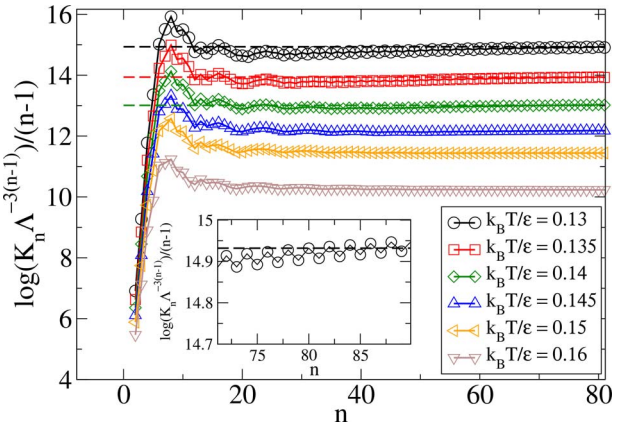

FIG. 11. $\log(K_n\Lambda^{-3(n-1)})/(n-1)$ for different temperatures. The dashed lines indicate equilibrium constants calculated from Eq. (18), with $v_b = 6.2\times10^{-6}\sigma^3$, and $\Delta U = -3.5\epsilon$. The inset shows the small oscillations associated with the addition of one particle to a tube.

Knowing that the energy of adding a particle to a tube corresponds to the formation of seven bonds (so that $\Delta U = -3.5\epsilon$ in Eq. (18)), it is possible to obtain the best fit value for the entropic term (v_b), yielding $v_b \approx 6.2\times10^{-6}\sigma^3$. The corresponding values for K_n for the three lowest values of T are reported as lines in Fig. 11 and properly model the numerical data. For smaller n, a significant n-dependence is still present. In this region, K_n shows oscillations with a periodicity of $\Delta n = 8$, signaling the cluster sizes which compete with tube formation. It is also interesting to note that for these clusters, the $\log(K_n\Lambda^{-3(n-1)})/(n-1)$ values are greater than in the $n\to\infty$ limit. This indicates that the free energy per particle is lower in small clusters, despite the fact that the potential energy per particle is lower for tubes (see Fig. 5). Therefore, the small clusters are significantly stabilized by their internal entropy. The crossover from disorganized clusters into straight tubes below T_x, clearly shown in Fig. 4, can thus be seen as a competition between two different free-energy local minima, one stabilized by entropy and one by energy. The large entropic difference between these two minima ensures that tubes only form at low temperatures. At this point, the large total change in energy associated with transforming a number of small clusters into a large tube, as compared to the thermal energy scale k_BT causes the free-energy difference between the two states to be very sensitive to small changes in temperature. This results in the sharp crossover seen in the energy and average cluster size as a function of temperature (Fig. 7), and the sudden appearance of tubular structures at T_x (Fig. 9).

IV. CONCLUSIONS

In this article, we have performed an in-depth analysis of a self-assembly process that takes place in a simple model system of one-patch colloids with a single attractive patch. In the appropriate density and temperature window, the particles form tubular structures that grow extremely long.

The specific tube-like cluster topology is imposed by the geometrical constraints that limit the number of bonds each patch can form. The tubes grow straight, without branching. Using direct NVT and single-cluster simulations, we have revealed that there is a well-defined temperature at which tubes start to appear, after which the average cluster size grows linearly with density, a clear fingerprint of cooperative polymerization.[17,21–24]

The possibility of numerically evaluating, with high accuracy, the partition functions of clusters of different size, made available by the recent development of accurate numerical methodologies,[66,68] allows us to quantify precisely the polymerization process and investigate the microscopic origin of the cooperative behavior. As previously assumed in the analysis of supramolecular ordering, the transition originates from the competition of two different local structures, differing in their energy and in their entropy. For a limited range of sizes, at low T, the partition function probes configurations associated with both tubes as well as more disordered clusters. The competition between these two different self-assembly processes generates a two-step aggregation, characterized by a sudden increase in the number of tubes around a density-dependent crossover temperature.

This numerical investigation, the first of its genre, illustrates the microscopic mechanism behind cooperative polymerization. The ability to directly measure equilibrium reaction constants for a microscopic pairwise additive model which generates cooperative polymerization offers a novel way to extract equilibrium constants also in other interesting numerical self-assembly processes.[35,69] Finally, this work highlights the strong link between supramolecular assembly[70] and colloidal assembly and the possibility of transferring knowledge between these two, only apparently different, fields.

ACKNOWLEDGMENTS

The authors gratefully acknowledge funding from ERC-226207-PATCHYCOLLOIDS (Teun Vissers, Frank Smallenburg, and Gianmarco Munaò), ITN-234810-COMPLOIDS (Zdeněk Preisler), and MIUR-PRIN (Francesco Sciortino).

[1] G. Odian, *Principles of Polymerization* (John Wiley & Sons, 2004).
[2] K. Matyjaszewski and J. Xia, Chem. Rev. **101**, 2921–2990 (2001).
[3] V. C. Gibson and S. K. Spitzmesser, Chem. Rev. **103**, 283–316 (2003).
[4] N. M. G. Franssen, J. N. H. Reek, and B. de Bruin, Chem. Soc. Rev. **42**, 5809–5832 (2013).
[5] R. Saito, G. Dresselhaus, and M. S. Dresselhaus, *Physical Properties of Carbon Nanotubes* (Imperial College Press, London, 1998), Vol. 4.
[6] M. M. Shulaker, G. Hills, N. Patil, H. Wei, H.-Y. Chen, H.-S. Philip Wong, and S. Mitra, Nature (London) **501**, 526–530 (2013).
[7] T. Scheibel, R. Parthasarathy, G. Sawicki, X.-M. Lin, H. Jaeger, and S. L. Lindquist, Proc. Natl. Acad. Sci. U.S.A. **100**, 4527–4532 (2003).
[8] W.-F. Xue, S. W. Homans, and S. E. Radford, Proc. Natl. Acad. Sci. U.S.A. **105**, 8926–8931 (2008).
[9] Q. Meng, Y. Kou, X. Ma, Y. Liang, L. Guo, C. Ni, and K. Liu, Langmuir **28**, 5017 (2012).
[10] A. G. Daful, J. B. Avalos, and A. D. Mackie, Langmuir **28**, 3730 (2012).
[11] Y. A. Berlin, A. L. Burin, and M. A. Ratner, Superlatt. Microstruct. **28**, 241–252 (2000).
[12] C. De Michele, T. Bellini, and F. Sciortino, Macromolecules **45**, 1090–1106 (2012).
[13] H. R. Vutukuri, A. F. Demirörs, B. Peng, P. D. J. van Oostrum, A. Imhof, and A. van Blaaderen, Ang. Chem. **124**, 11411–11415 (2012).
[14] F. Smallenburg, H. R. Vutukuri, A. Imhof, A. van Blaaderen, and M. Dijkstra, J. Phys.: Condens. Matter **24**, 464113 (2012).
[15] S. C. Greer, Ann. Rev. Phys. Chem. **53**, 173 (2002).
[16] S. C. Greer, J. Phys. Chem. B **102**, 5413–5422 (1998).
[17] T. F. De Greef, M. M. Smulders, M. Wolffs, A. P. Schenning, R. P. Sijbesma, and E. Meijer, Chem. Rev. **109**, 5687–5754 (2009).
[18] F. Sciortino, E. Bianchi, J. F. Douglas, and P. Tartaglia, J. Chem. Phys. **126**, 194903 (2007).
[19] K. Liu, Z. Nie, N. Zhao, W. Li, M. Rubinstein, and E. Kumacheva, Science **329**, 197–200 (2010).
[20] M. E. Cates and S. J. Candau, J. Phys.: Condens. Matter **2**, 6869 (1990).
[21] R. Goldstein and L. Stryer, Biophys. J. **50**, 583–599 (1986).
[22] M. M. Smulders, M. M. Nieuwenhuizen, T. F. de Greef, P. van der Schoot, A. P. Schenning, and E. Meijer, Chem-Eur. J. **16**, 362–367 (2010).
[23] J. van Jaarsveld and P. van der Schoot, Macromolecules **40**, 2177–2185 (2007).
[24] J. F. Douglas, J. Dudowicz, and K. F. Freed, J. Chem. Phys. **128**, 224901 (2008).
[25] J. Stambaugh, K. V. Workum, J. F. Douglas, and W. Losert, Phys. Rev. E **72**, 031301 (2005).
[26] W. Knoben, N. A. M. Besseling, and M. A. Cohen Stuart, Macromolecules **39**, 2643–2653 (2006).
[27] G. Jackson, W. G. Chapman, and K. Gubbins, Mol. Phys. **65**, 1 (1988).
[28] K. V. Workum and J. F. Douglas, Phys. Rev. E **71**, 031502 (2005).
[29] K. Van Workum and J. F. Douglas, Phys. Rev. E **73**, 031502 (2006).
[30] J. Dudowicz, K. F. Freed, and J. F. Douglas, Phys. Rev. Lett. **92**, 045502 (2004).
[31] J. Dudowicz, K. F. Freed, and J. F. Douglas, J. Chem. Phys. **111**, 7116 (1999).
[32] J. Dudowicz, K. F. Freed, and J. F. Douglas, J. Chem. Phys. **119**, 12645–12666 (2003).
[33] I. G. Economou and M. D. Donohue, AIChE J. **37**, 1875–1894 (1991).
[34] J. Dudowicz, K. F. Freed, and J. F. Douglas, J. Chem. Phys. **113**, 434–446 (2000).
[35] B. Huisman, P. Bolhuis, and A. Fasolino, Phys. Rev. Lett. **100**, 188301 (2008).
[36] L. Bouteiller and P. van der Schoot, J. Am. Chem. Soc. **134**, 1363–1366 (2012).
[37] M. Roman, C. Cannizzo, T. Pinault, B. Isare, B. Andrioletti, P. van der Schoot, and L. Bouteiller, J. Am. Chem. Soc. **132**, 16818–16824 (2010).
[38] M. Bellot and L. Bouteiller, Langmuir **24**, 14176–14182 (2008).
[39] J. van Gestel, P. van der Schoot, and M. Michels, Langmuir **19**, 1375–1383 (2003).
[40] R. E. Harris, J. Phys. Chem. **74**, 3102–3111 (1970).
[41] J. C. Wheeler, S. J. Kennedy, and P. Pfeuty, Phys. Rev. Lett. **45**, 1748–1752 (1980).
[42] G. Gee, Trans. Faraday Soc. **48**, 515–526 (1952).
[43] F. Fairbrother, G. Gee, and G. T. Merrall, J. Polym. Sci. **16**, 459–469 (1955).
[44] J. A. Cuesta and R. P. Sear, Phys. Rev. E **65**, 031406 (2002).
[45] A. Wegner and J. Engel, Biophys. Chem. **3**, 215–225 (1975).
[46] F. Federiconi, P. Ausili, G. Fragneto, C. Ferrero, and P. Mariani, J. Phys. Chem. B **109**, 11037–11045 (2005).
[47] P. Mariani, F. Spinozzi, F. Federiconi, H. Amenitsch, L. Spindler, and I. Drevensek-Olenik, J. Phys. Chem. B **113**, 7934–7944 (2009).
[48] N. Kern and D. Frenkel, J. Chem. Phys. **118**, 9882–9889 (2003).
[49] W. Bol, Mol. Phys. **45**, 605–616 (1982).
[50] E. Bianchi, J. Largo, P. Tartaglia, E. Zaccarelli, and F. Sciortino, Phys. Rev. Lett. **97**, 168301 (2006).
[51] C. Vega, E. Sanz, J. L. F. Abascal, and E. G. Noya, J. Phys.: Condens. Matter **20**, 153101 (2008).
[52] F. Romano, P. Tartaglia, and F. Sciortino, J. Phys.: Condens. Matter **19**, 322101 (2007).
[53] Q. Chen, S. C. Bae, and S. Granick, Nature (London) **469**, 381–384 (2011).
[54] F. Romano and F. Sciortino, Soft Matter **7**, 5799–5804 (2011).
[55] E. G. Noya, C. Vega, J. P. K. Doye, and A. A. Louis, J. Chem. Phys. **132**, 234511 (2010).
[56] E. G. Noya, C. Vega, J. P. K. Doye, and A. A. Louis, J. Chem. Phys. **127**, 054501 (2007).
[57] E. G. Noya, M. M. Conde, and C. Vega, J. Chem. Phys. **129**, 104704 (2008).
[58] J. P. K. Doye, A. A. Louis, I.-C. Lin, L. R. Allen, E. G. Noya, A. W. Wilber, H. C. Kok, and R. Lyus, Phys. Chem. Chem. Phys. **9**, 2197–2205 (2007).
[59] F. Romano, E. Sanz, P. Tartaglia, and F. Sciortino, J. Phys.: Condens. Matter **24**, 064113 (2012).

[60]F. Romano, E. Sanz, and F. Sciortino, J. Chem. Phys. **134**, 174502 (2011).
[61]T. Vissers, Z. Preisler, F. Smallenburg, M. Dijkstra, and F. Sciortino, J. Chem. Phys. **138**, 164505 (2013).
[62]F. Romano and F. Sciortino, Nat. Matter **10**, 171–173 (2011).
[63]F. Romano and F. Sciortino, Nat. Commun. **3**, 975 (2012).
[64]G. Munaó, Z. Preisler, T. Vissers, F. Smallenburg, and F. Sciortino, Soft Matter **9**, 2652 (2013).
[65]Z. Preisler, T. Vissers, F. Smallenburg, G. Munaò, and F. Sciortino, J. Phys. Chem. B **117**, 9540–9547 (2013).
[66]R. Fantoni, A. Giacometti, F. Sciortino, and G. Pastore, Soft Matter **7**, 2419–2427 (2011).
[67]R. Pool and P. G. Bolhuis, J. Phys. Chem. B **109**, 6650–6657 (2005).
[68]D. J. Kraft, R. Ni, F. Smallenburg, M. Hermes, K. Yoon, D. A. Weitz, A. van Blaaderen, J. Groenewold, M. Dijkstra, and W. K. Kegel, Proc. Natl. Acad. Sci. U.S.A. **109**, 10787–10792 (2012).
[69]Z.-W. Li, Z.-Y. Lu, Z.-Y. Sun, and L.-J. An, Soft Matter **8**, 6693–6697 (2012).
[70]L. Leibler, Prog. Polym. Sci. **30**, 898–914 (2005).